DESIGN, TEST, AND VERIFIACTION OF A REACTION WHEEL FOR CUBESATS

Zayed Alkatheeri, Abderrahim Nabi, Djamal Darfilal, Sean Swei, Elena Fantino

Department of Aerospace engineering, Khalifa University of Science and Technology, Abu Dhabi, United Arab Emirates

Email: {100063553, abderrahim.nabi, djamal.darfilal sean.swei, elena.fantino }@ku.ac.ae

Abstract

Khalifa University's initiatives in designing and constructing CubeSats for technology demonstration show a significant leap in advancing space capabilities. The ongoing project involves a 6U CubeSat destined for Low Earth Orbit (LEO) at YahSat space lab. This research primarily focuses on designing, testing, and developing a flight model reaction wheel for integration into the current 6U CubeSat mission at Khalifa University. The design phase involves careful analysis of key factors, such as flywheel design and motor selection from low-cost commercial of the shelf motors, with a primary focus on reducing the weight and size while maintaining optimal performance. Furthermore, a thorough modelling, simulation, and analysis of the reaction wheel are presented, using a Proportional Integral (PI) controller to illustrate the performance of the selected Brushless DC motor under flywheel loading conditions. The results showed that the reaction wheel performs within the expected behaviour proving the compatibility of the flywheel geometric properties at the operational speed and torque limits. Furthermore, the paper presents a miniaturized flight model reaction wheel with only 33mm in diameter, weighing under 38g, and capable of generating a maximum torque of 1.72mNm while storing 1.32mNms of angular momentum. At the hardware level, the reaction wheel is integrated with a PI controller circuit, initially tuned using a trial-and-error method. To validate the simulation study, functional tests were conducted, and the results are illustrated for comparison to show the performance of the reaction wheel at different operational modes considering all physical factors including friction and vibrations. The in-house development of the reaction wheel contributes to the space heritage of the United Arab Emirates in space systems technology.

Keywords: Reaction wheel Design; Satellite Attitude Control; ADCS; CubeSat; Flywheel

1. Introduction

Nanosatellites, known as CubeSats, with masses ranging from 1 kg to 10 kg have gained popularity for their affordability and versatility. CubeSats are designed in cube configurations, starting from a 1U size (10x10x10 cm) and expanding up to 12U. Beyond cost-effectiveness, CubeSats have demonstrated applications in earth observation, atmospheric studies, and technology demonstration. Precision pointing is crucial for CubeSat missions for various reasons, necessitating an Attitude Determination and Control System (ADCS). While various ADCS actuators are utilized, such as reaction wheels and magnetorquers; however, reaction wheels, with spinning flywheels, are preferred for maintaining CubeSat attitude. This paper proposes a cost-effective reaction wheel development methodology, including simulation tests by modelling the reaction wheel as a loaded DC-motor to simulate the system's performance using a PI-controller. The paper begins by presenting a thorough literature review of reaction wheel sizes to investigate the diversity of reaction wheel characteristics integrated in different satellite scales. Secondly, the paper presents a block diagram of a miniaturized flight model reaction wheel. The study also presents the hardware design and sizing of the proposed reaction

wheel. Furthermore, the paper illustrates the simulation and experimental results of the performance tests.

2. The-state-of-the art reaction wheels review

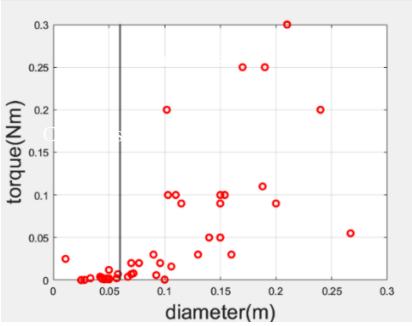

Figure 1: Torque versus diameter of reaction wheels.

The correlation between reaction wheels and satellite sizes is evident in Figure 1, which summarizes state-of-the-art reaction wheel models. The plot illustrates the mapping of these models based on torque output and maximum outer diameter. Reaction wheels with sizes below 6 cm, indicated by the dividing line find use in CubeSats, while larger ones are deployed in Small Satellites. Small Satellites, being physically larger than CubeSats, experience larger external disturbances, necessitating larger flywheels and more powerful motors to provide sufficient torque output to counter disturbance torques. In Figure 1 individual reaction wheels with sizes below 0.06m are used in CubeSats, these reaction wheels have masses in the range of 21g to 375g, such as Cube wheel Medium and Nano Avionics RW0, with masses 150g and 137g respectively [1,2]. Based on the review of collective wheel models the preferable size and mass of a reaction wheel for a CubeSat is smaller than 6 cm with a mass no more than 375g considering the size and mass margin of CubeSats.

3. Reaction wheel design

3.1 Disturbance model

The reaction wheel size is tied to the CubeSat's dimensions, determined by the flywheel and motor sizes. The flywheel's dimensions and mass are set by its maximum angular momentum capacity. Additionally, the reaction wheel must be able to generate a maximum torque that exceed the total torque from environmental disturbances. Based on factors such as 6U CubeSat geometry and orbital parameters, the magnitude of disturbance torques on the 6U CubeSat was computed and it is shown in table 2. The method of calculations is shown by Kumar [3].

Mass (kg)	12
Dimensions(cm)	36x24x12

Table 1: CubeSat specifications.

Orbital altitude (km)	500
Density of air (kg/m^3)	4.6×10^{-13}

Table 2: Orbital parameters.

The dominant sources of disturbance and the equations to model them are as follows:

Gravity gradient torque

$$T_g = \frac{3\mu}{2R^3}|\mathrm{I_y} - \mathrm{I_z}|sin(2\theta) \quad (1) \quad [3]$$

The CubeSat is a rectangular cuboid; therefore, the moment of inertias is given by the following equations:

$$\mathrm{I_y} = \frac{1}{12}\mathrm{m}(\mathrm{l}^2 + \mathrm{w}^2) \quad (2)$$

$$\mathrm{I_z} = \frac{1}{12}\mathrm{m}(\mathrm{h}^2 + \mathrm{w}^2) \quad (3)$$

The azimuthal angle is taken to be the maximum angular displacement from the z-axis which is $45\,\mathrm{deg}$. The orbital radius in km of the CubeSat is calculated by:

$$R = y + R_E \qquad (4)$$

Aerodynamic torque

The aerodynamic torque and force are calculated using the following equations respectively:

$$T_D = F_D r \quad (5)\ [3]$$

Where F_D is the drag force and is given by the following:

$$F_D = \frac{1}{2}\rho v^2 S C_D \quad (6)$$

The air density is obtained from a table containing data for density as a function of altitude [4]. The contact surface area is chosen to be the maximum surface area of the CubeSat to maximize the torque margin of the reaction wheels. The velocity of the CubeSat is computed using Newton's second law in orbital mechanics, by equating the gravitational to the centripetal force we obtain:

$$\frac{\mu}{R^2} = \frac{v^2}{R} \qquad (7)$$

We solve for v; the velocity of the CubeSat is:

$$v = \left(\frac{\mu}{R}\right)^{0.5} \qquad (8)$$

The accepted values for the drag coefficient C_D are between 2 and 2.6 [5][6]. The distance from the centre of mass to the centre of pressure is taken to be the maximum length on the CubeSat for the purposes of maximizing the magnitude of torque.

Solar radiation torque

The solar radiation torque is expressed by the following equation:

$$T_{sp} = \frac{F_s}{c} A_s (1 + q) \cos(i) R_{sp} \quad (9)\ [3]$$

The reflectance factor depends on the material structure of the surface the light illuminates. The accepted value of the reflectance factor is 0.6 [7] [8]. The force applied at a point is reduced by the cosine of the incident angle i, since the goal is to maximize the torque an angle of 0 degree is chosen. Furthermore, the distance from the solar center of pressure to the center of mass represents the moment arm and is taken to be the longest side length of the CubeSat.

Magnetic torque

The magnetic torque is computed by the equation:

$$T_m = DB \quad (10)\ [3]$$

The magnetic field profile of earth is approximated by:

$$B = \frac{2M}{R^3} \quad (11) \quad [3]$$

Table 3 and 4 show the definitions of the parameters from equation 1 to 11 and the selected values for the constant parameters respectively.

μ	Gravitational parameter
I_y	Moment of inertia about the y-axis of the CubeSat.
I_z	Moment of inertia about the z-axis of the CubeSat.
θ	Azimuthal angle of the CubeSat.
F_D	Drag force

r	Distance from center of mass of the CubeSat to the center of pressure.
F_s	Solar constant
c	Speed of light
A_s	Surface area
q	Reflectance
i	Angle of incidence
R_{sp}	Distance from center of mass of the CubeSat to the center of solar pressure.
D	Residual magnetic dipole
B	Magnetic field profile

Table 3: Parameters definition.

Reflectance (q)	0.6
Drag coefficient (C_D)	2
Earth magnetic moment (M) (Tm^3)	47.96×10^{-15}
Residual magnetic dipole (D) (Am^2)	0.01

Table 4: Parameter values.

Gravity gradient (nNm)	132.71
Solar radiation(nNm)	114.87
Aerodynamic drag (nNm)	429.45
Magnetic torque (nNm)	490.78
Total (μNm)	1.17

Table 4: disturbance torque magnitudes.

3.2 Hardware design

Flywheels on CubeSats, crucial for storing angular momentum, benefit from using high-density materials like stainless steel. Despite being among the heaviest components in reaction wheels, efforts focus on design modifications to minimize mass. The design criteria consider manufacturing challenges, the mass-to-momentum ratio, and time efficiency. The simplest wheel geometry, a flat disk, reduces imbalance risks but may not optimize the inertia-to-mass ratio. Alternative designs, such as wheels with internal spokes or a main disk with a peripheral ring, are explored. The hollowed surface design efficiently distributes mass at the edges, enhancing angular momentum storage with less mass. For protection from radiation and thermal effects, a lightweight and strong stainless steel 304 housing shields the entire system, including the flywheel, motor, and bearing, combatting radiation and thermal effects. With a hollow cylinder shape and circular base, the housing attaches to the supporting plate via bolts, ensuring stability. The plate, also made of 304 stainless steel, supports the entire system with a high strength-to-weight ratio. Sized to match the housing's outer diameter, the plate ensures rigidity and minimizes the risk of structural failure. Bolts with a diameter twice the thickness of the housing base secure the housing to the plate, providing stability. The lower limit on the flywheel's dimensions is determined by the required angular momentum for a 6U CubeSat to maintain attitude for at least 1/6th of its orbital period

$$H_{req} = \frac{\tau_{max} T}{6} \quad (12)$$

Considering τ_{max} as the total torque from table 2, and the CubeSat's altitude at 500 km yielding an orbital period of T ~ 5668 s, the minimum angular momentum is calculated as 1.1 mNms. The motor selection is based on both the angular momentum requirements for the reaction wheel and ease integration with the CubeSat.

The chosen motor has a maximum speed of 40,000 rpm, allowing the determination of the minimum flywheel moment of inertia as $0.2 \times 10^{-6} kgm^2$. Achieving this requires designing a flywheel with dimensions: outer diameter of 17 mm, height of 3.5 mm, and internal diameter of 10 mm.

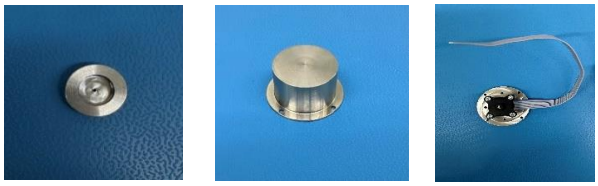

Figure 2: Reaction wheel components.

4. Performance tests

The reaction wheel is now set to begin performance tests to examine its limitations and operations at different inputs. The response of the reaction wheel to an input will reflect on the overall performance. The testing phase consists of a range of modes that the reaction wheel operates on, to test its response to different inputs. The first performance tests allow us to measure the saturation speed and torque, which are essential quantities that contribute to the functional operation. The flywheel is accelerated anti-clockwise until it reaches the maximum speed setpoint. Once reached, the reaction wheel is exposed to the same setpoint but in the opposite direction (Clockwise) to obtain the torque availability at a positive speed range. Finally, the reaction wheel is driven to rest to obtain the torque availability at a negative speed range. The saturation speed determines the saturation angular momentum of the reaction wheel. Once measured it can be compared with the calculated required angular momentum. The saturation torque is the maximum torque beyond which the motor cannot produce more torque. Estimating the saturation torque bounds will determine if the reaction wheel satisfies the requirement by providing a larger torque than the maximum disturbance torque.

Furthermore, the performance tests include operating the reaction wheel at different speeds. This can be done using a ramp input. One can observe the velocity response of the reaction wheel at different speeds and how the torque varies. Simulink models for the performance tests were designed. The method of the actual experimental testing follows the same approach as the simulation. The speed controller of the reaction wheel is adjusted to a certain configuration which defines the controller gains, maximum voltage and speed, and the method of control.

Parameter	Value
Maximum motor speed (rpm)	40000
Maximum motor voltage (V)	27
PI gains	$K_P = 750\ K_I = 0.13$
Motor control method	PWM signals

Table 5: Speed controller configuration.

During the experimental testing of the reaction wheel, an Arduino microcontroller was employed to compute the speed set point based on the duty cycle of the pulse-width modulation (PWM) signal. This approach allowed for precise control over the rotational speed of the reaction wheel. Subsequently, torque boundary plots were obtained for both step and ramp inputs. These plots provide valuable insights into the torque characteristics of the reaction wheel under different operating conditions. Analysing the torque response to step and ramp inputs offers a comprehensive understanding of the system's dynamic behaviour and performance. By comparing the experimental results with theoretical models and simulation data, a thorough assessment of the reaction wheel's functionality and response can be achieved.

4.1 Simulink model

The performance testing pushes the reaction wheel to its extreme limits to examine the conditions of the system at its highest risk. However, reaction wheels do not operate near the extreme points, a margin of safety is left to avoid overheating and overpower consumption of the motor. The torque generated by the motor is computed using an equation from the specification sheet of the motor, relating the torque output τ, speed-torque gradient $\frac{\Delta n}{\Delta \tau}$, setpoint speed $n_{setpoint}$, and the final speed reached by the reaction wheel n. The equation is expressed as follows:

$$\tau = \frac{\Delta n}{\Delta \tau}(n_{setpoint} - n) \quad (13)\ [9]$$

Where $\frac{\Delta n}{\Delta \tau} = 1734 \frac{rpm}{mNm}$, the speed-torque gradient is constant whose value is determined experimentally by the manufacturer, and it depends on the motor characteristics. A Simulink model is built to simulate the reaction wheel and verify the experimental results obtained from the testing. Equation (13) is valid if and only if the speed-torque gradient is not zero, which is true if the reaction wheel is exposed to a step input giving a non-linear speed curve.

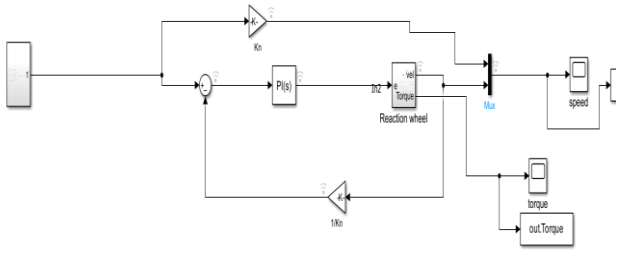

Figure 3: Reaction wheel model exposed step inputs.

$K_n\ (min^{-1}/V)$	1339
$K\ (min/rad)$	$\frac{60}{2\pi}$
$Setpoint\ (rpm)$	30000

Table 6: Motor parameters.

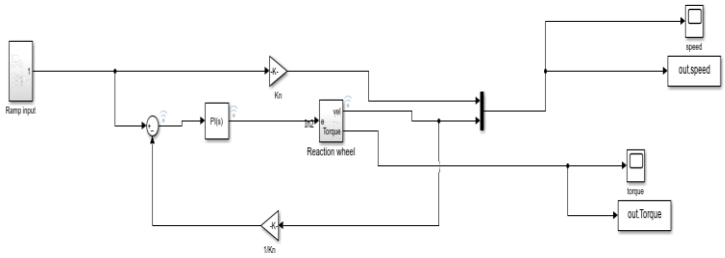

Figure 4: Reaction wheel model exposed ramp inputs.

4.2 Preliminary results

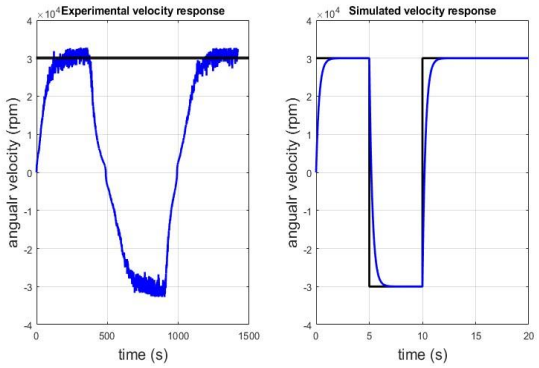

Figure 5: Time series plot of speed response to step inputs.

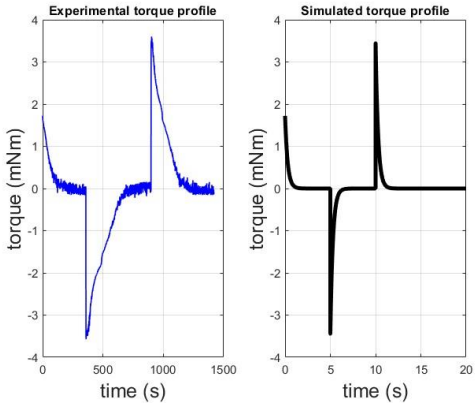

Figure 6: Time series plot of torque response to step inputs.

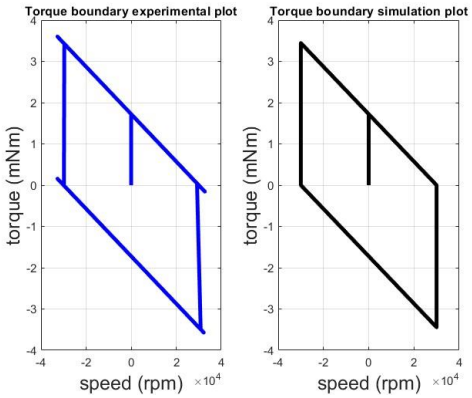

Figure 7: Torque boundary to step inputs.

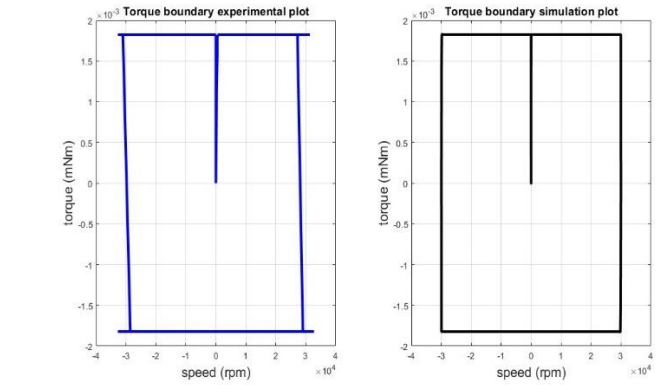

Figure 10: Time series plot of torque response to ramp inputs.

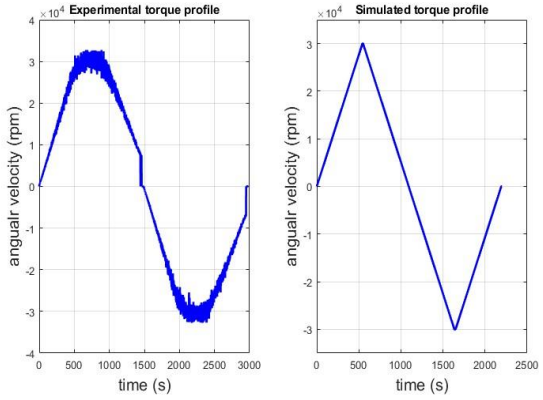

Figure 8: Time series plot of speed response to ramp inputs.

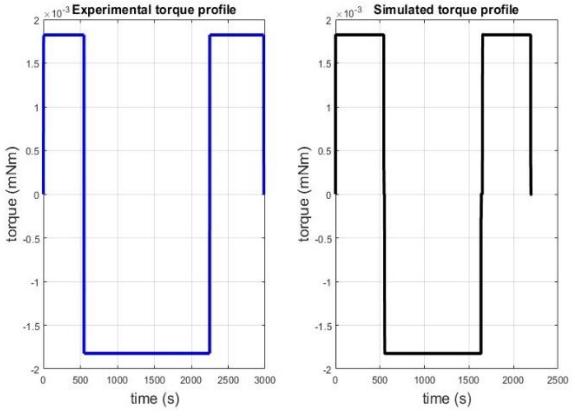

Figure 9: Time series plot of torque response to ramp inputs.

5. Discussion

The reaction wheel is subjected to the maximum voltage from the source, resulting in maximum torque generation across all operational speeds. The torque boundary plot, which displays saturation torque and speed, is particularly insightful. Figure 7 presents experimental results compared to simulation results of torque at various speeds under maximum step input conditions. Initially, the reaction wheel generates 1.72 mNm of torque at zero speed before accelerating. During acceleration, the torque decreases but remains positive until the speed reaches 30,000 rpm and the torque drops to zero. With the system exposed to the positive maximum voltage, the reaction wheel stabilizes at a constant maximum speed, indicating its saturation speed. Furthermore, the reaction wheel model is tested under negative maximum voltage to observe the response at negative torque values. Similar behaviour is observed, except the maximum torque is double the initial torque response as expected. Prior to applying negative maximum voltage, the reaction wheel rotates at its saturation speed. The subsequent application of negative maximum voltage first generates -1.72 mNm to reduce the speed to zero, followed by another -1.72 mNm to accelerate the reaction wheel in the opposite direction, totalling -3.44 mNm. The reaction wheel then achieves

its saturation speed in the opposite direction. This testing phase allows for an analysis of the reaction wheel's performance at various stages. Initially, negative maximum voltage reveals how effectively the reaction wheel can reduce and reverse the flywheel's speed from maximum positive to maximum negative, reflecting control performance. To complete the performance assessment, the motor's behaviour is explored as the flywheel's speed decreases to zero and accelerates back to positive saturation speed. Ultimately, a comprehensive closed-loop plot of torque and speed limits is created, demonstrating the developed reaction wheel's capabilities. In the second phase of testing, the reaction wheel is subjected to a ramp input, and the response is monitored until saturation. This phase examines the reaction wheel's performance at constant torque, gradually accelerating to positive saturation speed, reversing direction to negative saturation, and then returning to zero. The Simulink model used for this test is shown in Figure 4. During this operation, the reaction wheel generates constant torque, as illustrated in Figure 10. At zero speed, the reaction wheel generates 0.0018 mNm of torque, maintaining this magnitude until angular momentum saturates at maximum speed. The torque then reverses, as shown in Figure 8, which details the velocity response. Consequently, the ramp input tests provide a thorough evaluation of the reaction wheel's capability across all speed operating points.

6. Conclusions

The reaction wheel's performance in different modes was verified through various tests, including exposure to maximum and gradual voltage inputs. Additionally, a simplified reaction wheel model with a PI-controller was validated based on the experimental findings.

References

[1] "GEN 1 SENSORS & ACTUATORS," Cubespace

[2] "4RW0 - NanoAvionics | Reaction Wheel."

[3] S. Kumar, D. Sahay, S. R. Hegde, S. Sandya, A. K. Jha and T. C. Mahalingesh, "Design and development of 3-axis reaction wheel for STUDSAT-2," 2015 IEEE Aerospace Conference, Big Sky, MT, USA, 2015, pp. 1-13, doi: 10.1109/AERO.2015.711918.

[4] "Properties of standard atmosphere." http://www.braeunig.us/space/atmos.htm

[5] NATIONAL AERONAUTICS AND SPACE ADMINISTRATION, SPACE CRAFT AERODYNAMIC TORQUES NASA SPACE VEHICLE DESIGN CRITERIA (GUIDANCE AND CONTROL). 1971. [Online]. Available: https://ntrs.nasa.gov/api/citations/19710016459/downloads/19710016459.pdf

[6] D. Oltrogge and K. Leveque, "An Evaluation of CubeSat Orbital Decay," *AIAA/USU Conference on Small Satellites, 2011*, Aug. 2011, [Online]. Available: http://www.agi.com/downloads/resources/white-papers/20110808_SmallSat_CubeSat_Orbit_Lifetime_10.pdf

[7] NATIONAL AERONAUTICS AND SPACE ADMINISTRATION, *SPACECRAFT RADIATION TORQUES NASA SPACE VEHICLE DESIGN CRITERIA (GUIDANCE AND CONTROL)*. 1969. [Online]. Available:https://ntrs.nasa.gov/api/citations/19710014836/downloads/19710014836.pdf

[8] J. R. Wertz, *Spacecraft attitude determination and control*. 1978. doi: 10.1007/978-94-009-9907-7.

[9] *Motor calculations for coreless Brush DC Motors | Tutorial*. (n.d.). Dr. Fritz Faulhaber GmbH & Co. KG. https://www.faulhaber.com/en/know-how/tutorials/dc-motor-tutorial-motor-calculations-for-coreless-brush-dc-motors/

[10] *Microvibration test bench for tiny reaction wheels | TU Delft Repository*. (n.d.). https://repository.tudelft.nl/record/uuid:e04fab02-bfa6-47f5-b9be-1e85b2abf416